Sixth International Symposium on Turbulence and Shear Flow Phenomena
Seoul, Korea, 22-24 June 2009

LES APPROACH COUPLED WITH STOCHASTIC FORCING OF SUBGRID ACCELERATION IN COMPUTATION OF A HIGH REYNOLDS NUMBER CHANNEL FLOW

Rémi Zamansky, Ivana Vinkovic and Mikhael Gorokhovski
Laboratoire de Mécanique des Fluides et d'Acoustique (LMFA)
CNRS UMR 5509, Ecole Centrale de Lyon, Université Claude Bernard Lyon 1
69134 Ecully Cedex, France
remi.zamansky@ec-lyon.fr, ivana.vinkovic@ec-lyon.fr, mikhael.gorokhovski@ec-lyon.fr

ABSTRACT

In this paper, the non-filtered velocity field in a well-developed turbulent channel flow is simulated in the framework of LES-SSAM (stochastic subgrid acceleration model), Sabelnikov et al. (2007). A new stochastic subgrid scale (SGS) model is proposed. This model introduces explicitly the cross-channel correlation of subgrid velocity gradients and includes two parameters: the Reynolds number based on the friction velocity, and the channel half-width. The objective is to assess the capability of this model in comparison to the standard large-eddy simulation (LES) and to direct numerical simulation (DNS).

INTRODUCTION

The structure of well-developed turbulent wall layer in the channel flow is highly intermittent. Close to the wall, the low-speed regions are interleaved with tiny zones of high-speed motion. The main role in this intermittency is attributed to quasi-streamwise vortices formed in the near-wall layer (Kaftori et al., 1994; Adrian et al., 2000; Tomkins and Adrian, 2003). Their anisotropic dynamics are Reynolds-number dependent. Sweeps from the outer layer toward the wall induce strong variations of the wall-normal velocity. The cross-channel correlation in the turbulent velocity field is amplified by merging of near-wall small-scale structures and their eruptions towards the outer region (Jiménez et al. 2004; Hutchins and Marusic, 2007; Toh and Itano., 2005).

It has been shown that LES without model may reproduce accurately highly intermittent turbulent structures near the wall. However this requires excessively expensive grid resolution. Then for a high Reynolds number channel flow, the LES at moderate resolution has to be combined with a SGS model for the non-resolved turbulent motion. The majority of SGS models are focused on simulation of turbulent stresses generated by the non-resolved velocity field (Meneveau and Katz, 2000; Domaradzki and Adams, 2002; Park and Mahesh, 2008). In these models the structure of subgrid flow is supposed to be independent of the Reynolds number, *i.e.*, to be not intermittent. Therefore the approach recently proposed by Sabelnikov et al. (2007) is focused directly on the stochastic modeling of the subgrid acceleration (LES-SSAM).

It was shown, by Kolmogorov's scaling, that, for a given filter width Δ, the non-resolved acceleration may be substantially greater than the resolved acceleration: $(\overline{a}_k\overline{a}_k)/(a'_i a'_i) \approx (\eta/\Delta)^{2/3}$, where $\overline{a}_k$ and a'_i represent resolved and non-resolved accelerations and $\eta = L/Re_L^{3/4}$ is the Kolmogorov's length scale. This implies that in any SGS model, which is aimed to introduce the intermittency effects, the non-resolved acceleration must be a key variable. This motivated us to set up a new stochastic model for the subgrid acceleration of wall bounded flow. The aim of this paper is to assess the capability of the new model to reproduce the near-wall behavior compared to a standard LES and DNS.

LES-SSAM APPROACH AND MODEL FORMULATION

In the LES-SSAM framework of Sabelnikov et al. (2007), it is consider that the total instantaneous acceleration, governed by the Navier-Stokes equations, can be represented by the sum of two parts: $a_i = \overline{a}_i + a'_i$. The first part represents the spatially filtered total acceleration: $\overline{a}_i = \frac{\partial \overline{u}_i}{\partial t} + \frac{\partial \overline{u_k u_i}}{\partial x_k}$, and is equivalent, with spatial filtering of the Navier-Stokes equations, to:

$$\begin{aligned} \overline{a}_i \equiv \overline{\frac{du_i}{dt}} &= -\frac{1}{\rho}\frac{\partial \overline{p}}{\partial x_i} + \nu \Delta \overline{u}_i \\ \frac{\partial \overline{u}_k}{\partial x_k} &= 0 \end{aligned} \qquad (1)$$

with ν the kinematic viscosity. The second part is associated with the total acceleration in the residual field:

$$\begin{aligned} a'_i \equiv \left(\frac{du_i}{dt}\right)' &= -\frac{1}{\rho}\frac{\partial p'}{\partial x_i} + \nu \Delta u'_i \\ \frac{\partial u'_k}{\partial x_k} &= 0 \end{aligned} \qquad (2)$$

where $a'_i = \frac{\partial u'_i}{\partial t} + \frac{\partial u_k u_i - \overline{u_k u_i}}{\partial x_k}$. Both equations need to be modeled. In the LES-SSAM approach, eq. (1) is modeled in the framework of the classical LES approach, and a'_i is considered as a stochastic variable. The resulting model-equation, which reconstructs an approximation for the non-filtered velocity field, writes then as:

$$\begin{aligned} \frac{\partial \hat{u}_i}{\partial t} + \hat{u}_k \frac{\partial \hat{u}_i}{\partial x_k} &= -\frac{1}{\rho}\frac{\partial \hat{p}}{\partial x_i} \\ &+ \frac{\partial}{\partial x_k}(\nu + \nu_t)\left(\frac{\partial \hat{u}_i}{\partial x_k} + \frac{\partial \hat{u}_k}{\partial x_i}\right) + \hat{a}'_i \\ \frac{\partial \hat{u}_k}{\partial x_k} &= 0 \end{aligned} \qquad (3)$$

where $\hat{\bullet}$ represents a synthetic field and ν_{turb} is given by the Smagorinsky subgrid model.

For further development of the LES-SSAM approach, we propose a new model for the non-resolved acceleration $\hat{a'}_i$. We introduce the separation of variables for the non-resolved acceleration $\hat{a}'_i$. On the basis of our DNS for turbulent channel flow (see table 1) and experiences (Mordant et al. 2004;

Lee et al., 2004; Mordant et al., 2002), $|a|$, the modulus of the subgrid acceleration and e_i its orientation, are two independent random variables, characterized by long memory and rapid decorrelation, respectively. Then the non-resolved acceleration is written as:

$$\hat{a}'_i = |a| e_i \tag{4}$$

For $|a|$, our proposal is to emulate the modulus of the non-resolved acceleration in the following form:

$$|a| = f \Delta u_*^2 / \nu \tag{5}$$

where Δ is the characteristic cell size and u_* the friction velocity, $u_*^2/\nu \equiv \frac{\partial u}{\partial y}|_{\text{wall}}$; so $\Delta u_\tau^2/\nu$ will be considered as a typical normal to wall velocity increment in the near to wall region, and f is the subgrid frequency, considered as a stochastic variable. The frequency f is supposed to have a stochastic evolution from the wall to the outer flow driven by the non-dimensional parameter τ defined as follows:

$$\tau = -ln\left(\frac{h-y}{h}\right) \tag{6}$$

where h is the channel half-width, and y is the wall distance ($y = 0 : \tau = 0$ and $y \to h : \tau \to \infty$). The near-wall region is characterized by strong velocity gradients (high values of f), which decrease in mean toward the outer flow through the highly intermittent boundary layer. Thereby we assumed that with increasing of the normal distance from the wall, the frequency f is changing by a random independent multiplier α ($0 < \alpha < 1$), governed by distribution $q(\alpha)$, $\int_0^1 q(\alpha) d\alpha = 1$, which is in principle unknown. In other words, we apply the fragmentation stochastic process under scaling symmetry for the frequency f. From Gorokhovski and Saveliev (2008), we derive the following stochastic equation corresponding to this process:

$$df = \left(\langle ln\alpha \rangle + \langle ln^2\alpha \rangle/2\right) f d\tau + \sqrt{\langle ln^2\alpha \rangle/2} f dW(\tau) \tag{7}$$

where $\langle ln^k\alpha \rangle = \int_0^1 q(\alpha) ln^k\alpha d\alpha$; $k = 1, 2$, and $dW(\tau)$ is the Wiener process ($\langle dW(\tau) \rangle = 0$ and $\langle dW(\tau)^2 \rangle = d\tau$). In the present study, parameters are chosen in the following form:

$$-\langle ln\alpha \rangle = \langle ln^2\alpha \rangle = Re_+^{1/3} \tag{8}$$

where Re_+ is the Reynolds number, based on the friction velocity u_*. The starting condition, $\tau = 0$, for this stochastic process (the first grid cell on the wall) is given as follows. We introduce the mean value of frequency at the wall $f_+ = \lambda/u_*$, where λ is determined, as a Taylor-like scale, which can be estimated by the Kolmogorov's scaling in the framework of definitions of wall parameters. The Reynolds number, based on friction velocity, is $Re_+ = u_* h/\nu = h/y_0 \approx Re_h^{3/4}$ where y_0 is the thickness of the viscous layer, and Re_h is the Reynolds number based on the center-line velocity. One then yields: $\lambda \approx h Re_h^{-1/2} \approx h Re_+^{-2/3}$. Similar to Kolmogorov-Oboukhov 62, the starting condition for the random path given by eq. (7) is sampled from the stationary log-normal distribution of f/f_+:

$$P_0\left(f/f_+\right) = \frac{f_+}{f\sqrt{2\pi\sigma^2}} e^{-\frac{(ln(f/f_+) - \mu)^2}{2\sigma^2}} \tag{9}$$

If $\sigma^2 = \ln 2$ and $\mu = -\frac{1}{2}\sigma^2$, then $\langle f \rangle = (\langle f^2 \rangle - \langle f \rangle^2)^{1/2} = f_+$. This stochastic process will relax f from a log-normal distribution at the wall ($\tau = 0$) to the power distribution as the distance to the wall increases ($\tau \to \infty$). The evolution through the channel, for distributions of the frequency predicted by the stochastic equation can be compared with the evolution of the frequency computed from DNS, via eq. (5). According to fig. 1a SSAM ensures a good relaxation of the frequency, as the distance to the wall increases.

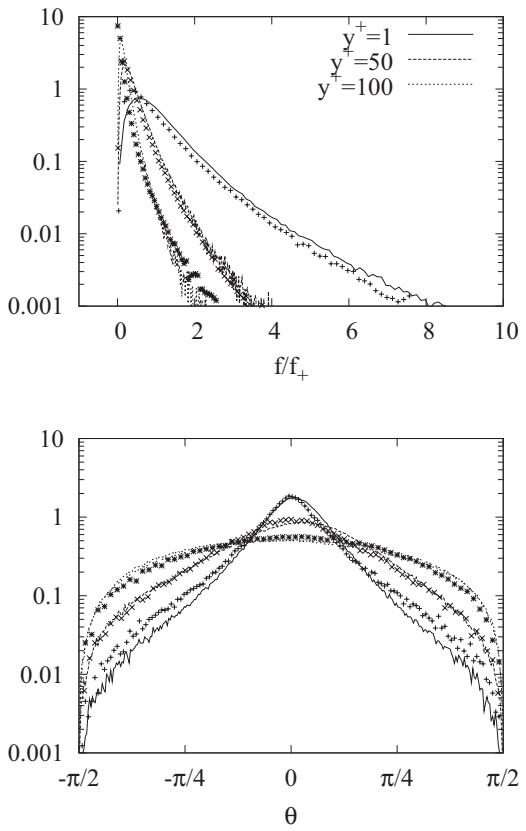

Figure 1: a: Distribution of f/f_+ from SSAM (cross) and comparison with DNS (line) at $Re_+ = 590$, for several distances from the wall. b: Distribution of θ for small scale acceleration from DNS (line) and from SSAM (cross), for $Re_+ = 590$, and for several distances from the wall ($y+ = 3$, $y+ = 10$ and $y+ = 30$).

In order to emulate the orientation vector of the subgrid scale acceleration, e_i, we consider a random walk evolving on the surface of a sphere of unity radius. The direction of this vector is defined by two stochastic variables which are longitude ϕ and latitude θ:

$$\begin{cases} e_x &= cos(\theta)\cos(\phi) \\ e_y &= \sin(\theta) \\ e_z &= cos(\theta)\sin(\phi) \end{cases} \tag{10}$$

The ϕ angle characterizes the direction in the streamwise-spanwise (x, z) plan, and the other one, θ, defines the orientation in relation to the normal to wall direction ($\theta = 0$ means acceleration is parallel to the wall, and $\theta = \pm\pi/2$ means acceleration is normal to the wall), fig 2. It is seen from DNS (fig. 1b) that the orientation vector relaxes toward isotropy with increasing distance from the wall. In the case of full isotropy, the distributions of θ and ϕ are respectively given by $P_{isotropic}(\theta) = \cos(\theta)/2$ and $P_{isotropic}(\phi) = \pi/2$. In order to represent this tendency towards isotropy, we implement the Kubo oscilator with a real coefficient α as

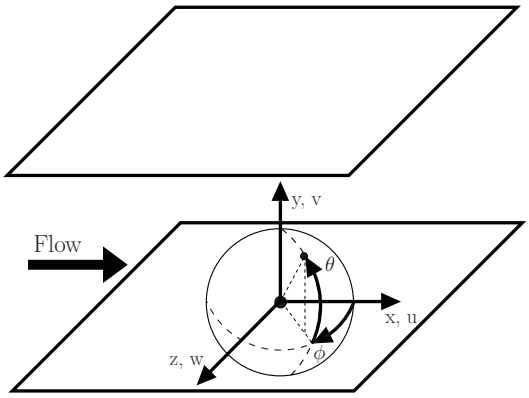

Figure 2: Coordinate system.

random motion on the sphere. This motion will defines the evolution of the unit vector e_i. Each position increment of the random walk is given by $\zeta = \alpha dW(\tau)$, with :

$$\alpha = \sqrt{\frac{\ln Re_+}{2}} \tag{11}$$

and the direction β at each time step is chosen randomly from the uniform distribution. The position increment ($d\theta = \theta_{i+1} - \theta_i, d\phi = \phi_{i+1} - \phi_i$) is given according to:

$$\begin{array}{rcl} \theta_{i+1} & = & \sin^{-1}(\sin\theta_i \cos\zeta + \cos\theta_i \sin\zeta \cos\beta) \\ d\phi & = & \arg(\gamma) \\ \Re(\gamma) & = & \sin\beta \sin\zeta \cos\theta_i \\ \Im(\gamma) & = & \cos\zeta - \sin\theta_i \sin\theta_{i+1} \end{array} \tag{12}$$

where γ is a complex number and $\Re(\gamma)$ and $\Im(\gamma)$ are its real and imaginary part, respectively. As τ increases the random walk covers all the surface of the sphere. This process is initiated on the wall with:

$$\left\{ \begin{array}{rcll} P_\theta(\theta, \tau = 0) & = & \delta(\theta) & \\ P_\phi(\phi, \tau = 0) & = & 1/2\pi & \text{if } 0 \leq \phi < 2\pi \end{array} \right. \tag{13}$$

where P_θ and P_ϕ are the distribution of θ and ϕ respectively, and δ is the Dirac distribution. The initial condition (13) is coherent with DNS. On fig. 1b we present the evolution of the distribution of θ given by eq. 6, eq. 11, eq. 12 and eq. 13 and the one computed from the small-scale acceleration of DNS. Good agreement with the DNS is achieved.

NUMERICAL RESULTS AND DISCUSSION

In order to make *a posteriori* tests of this subgrid scale model for acceleration we ran simulations of a pressure driven turbulent channel flow for three Reynolds numbers: $Re_+ = 590$, 1000 et 2000. We used a pseudo-spectral method with integration in time by the explicit Adam-Basforth algorithm for convective terms, and by the semi-implicit algorithm for diffusion terms. A rotational form is used for non-linear terms in order to ensure the conservation of energy. Periodic boundary conditions were applied along the streamwise (x) and the spanwise (z) directions, whereas the no-slip boundary condition was imposed on the walls.

The results of LES-SSAM tests have been compared with standard LES and DNS. We used our own DNS data as well as the DNS data from Moser et al. (1999) and from Hoyas and Jiménez (2008). For LES and LES-SSAM simulations the classical Smagorinsky model with a wall damping function for the turbulent viscosity has been applied (Sagaut, 2002):

$$\begin{array}{rcl} \nu_{turb} & = & (C_s \Delta f_{VD})^2 |S| \\ |S| & = & (2 S_{ij} S_{ij})^{1/2} \\ f_{VD} & = & 1 - e^{-y/A} \end{array} \tag{14}$$

with C_s the Smagorinsky constant, $\Delta = (\Delta x \times \Delta y \times \Delta z)^{1/3}$ the typical cell size, $S_{ij} = \frac{1}{2}\left(\frac{\partial \overline{u}_i}{\partial x_j} + \frac{\partial \overline{u}_j}{\partial x_i}\right)$ the resolved rate of strain tensor, f_{VD} the Van Driest function and A the constant controlling the damping of f_{VD}. The constant A is computed in order to fulfill the suggestion of Shur et al. (2008) for the subgrid length-scale ℓ definition: $\ell = \min(y, \Delta)$, y is the distance to the nearest wall. We choose A such that $\Delta f_{VD} \sim \min(y, \Delta)$ by least square regression: $\frac{d}{dA}\left[\sum_i \left((\min(y_i, \Delta_i))^2 - (\Delta_i f_{VD,i})^2\right)\right] = 0$, where the subscript i denote the i^{th} cell from the wall. The parameters used for these simulations are summarized in table 1.

Note that in this code, Reynolds number are imposed via the setting of ν and $-\frac{1}{\rho}\frac{\partial P}{\partial x_i}$ (the mean pressure gradient). One may use Dean's correlation (Dean, 1978): $\nu = 0.110 U_c h Re_+^{-1.1296}$ and $-\frac{1}{\rho}\frac{\partial P}{\partial x_i} = Re_+^2 \nu^2 / h^3$, with U_c the center-line velocity, to choose suitable values. As shown in table 1, the Reynolds numbers computed from LES-SSAM are closer to the DNS than the ones computed by LES. For a given set of parameters (ν and $-\frac{1}{\rho}\frac{\partial P}{\partial x_i}$), LES-SSAM improves both center-line velocity and mass flow rate estimations.

For simplicity reasons, in the following, we only present the LES-SSAM, LES and DNS comparison for simulations with a $64 \times 65 \times 64$ grid for the three Reynolds numbers. It should be noted that for finer resolutions the differences between LES-SSAM and standard LES are less pronounced, but still present.

Fig. 3 shows evolution of the mean velocity across the channel. As pointed out in table 1 it is clear that LES-SSAM improves mean flow rate estimation as well as center-line velocity prediction. Moreover the mean velocity profile follows the logarithmic law contrary to LES.

On fig. 4 profiles of the standard deviation for streamwise, spanwise and normal to wall velocities are also presented. Standard deviations of streamwise velocity are notably improved. The peak position obtained by LES-SSAM is closer to the DNS than the one obtained with LES. For the spanwise velocity standard deviation the improvement is less visible. However, note that the shape of the profile obtained by LES-SSAM is closer to the DNS one, even if it is overestimated. Finally, the normal to the wall velocity standard deviation is slightly improved in comparison with LES.

Fig. 5 illustrates the computation of turbulent and viscous stresses, $\tau_{turb} = -\rho\langle u'v'\rangle$ and $\tau_{visc} = -\rho\nu\langle\frac{\partial u}{\partial y}\rangle$, respectively ($\langle . \rangle$ denotes ensemble average). The results are presented as ratios $\tau_{turb}/(\tau_{turb} + \tau_{visc})$ and $\tau_{visc}/(\tau_{turb} + \tau_{visc})$. Here again the advantage of the LES-SSAM approach versus the classical LES is explicitly seen, and can be interpreted as a better estimation of momentum fluxes in the normal to the wall direction.

Velocity spectra are shown on fig. 6. From this figure we can see that the anomalous small scale (high wave number) damping inherent to LES can be reduced by LES-SSAM. Fig. 7 represents the evolution of the longitudinal autocorrelation coefficient for the streamwise velocity component along the channel. Improvement of the decorrelation length can be seen, indicating that integral length scale computed

Table 1: Summery of parameters used for numerical simulations

Name	Re_+	Re_c	$N_x \times N_y \times N_z$	$L_x \times L_y \times L_z$	$\Delta x^+ \times \Delta y^+ \times \Delta z^+$	C_s	A/h
DNS	587	12490	$384 \times 257 \times 384$	$\frac{3}{2}\pi h \times 2h \times \frac{3}{4}\pi h$	$7.2 \times (0.04 \sim 7.2) \times 3.6$	-	-
DNS[1]	587	12547	$384 \times 257 \times 384$	$2\pi h \times 2h \times \pi h$	$9.7 \times (0.04 \sim 7.2) \times 4.8$	-	-
LES	587	14160	$64 \times 65 \times 64$	$3\pi h \times 2h \times \pi h$	$87 \times (0.71 \sim 29) \times 29$	0.16	0.015
LES-SSAM	587	12760	$64 \times 65 \times 64$	$3\pi h \times 2h \times \pi h$	$87 \times (0.71 \sim 29) \times 29$	0.16	0.015
DNS	1000	22250	$512 \times 385 \times 512$	$\frac{4}{3}\pi h \times 2h \times \frac{2}{3}\pi h$	$8.2 \times (0.03 \sim 8.3) \times 4.1$	-	-
DNS[2]	934	20960	$3072 \times 385 \times 2304$	$8\pi h \times 2h \times 3\pi h$	$7.6 \times (0.06 \sim 7.6) \times 3.8$	-	-
LES	1000	25430	$96 \times 97 \times 96$	$3\pi h \times 2h \times \pi h$	$99 \times (0.53 \sim 33) \times 33$	0.16	0.009
LES-SSAM	1000	23380	$96 \times 97 \times 96$	$3\pi h \times 2h \times \pi h$	$99 \times (0.53 \sim 33) \times 33$	0.16	0.009
LES	1000	25500	$64 \times 65 \times 64$	$3\pi h \times 2h \times \pi h$	$147 \times (1.2 \sim 49) \times 49$	0.2	0.015
LES-SSAM	1000	23700	$64 \times 65 \times 64$	$3\pi h \times 2h \times \pi h$	$147 \times (1.2 \sim 49) \times 49$	0.2	0.015
DNS[2]	2003	48680	$6144 \times 633 \times 4608$	$8\pi h \times 2h \times 3\pi h$	$8.2 \times 8.9 \times 4.1$	-	-
LES	2000	49350	$128 \times 129 \times 128$	$3\pi h \times 2h \times \pi h$	$147 \times (0.60 \sim 49) \times 49$	0.16	0.006
LES-SSAM	2000	48950	$128 \times 129 \times 128$	$3\pi h \times 2h \times \pi h$	$147 \times (0.60 \sim 49) \times 49$	0.16	0.006
LES	2000	52640	$64 \times 65 \times 64$	$3\pi h \times 2h \times \pi h$	$295 \times (2.4 \sim 98) \times 98$	0.2	0.015
LES-SSAM	2000	49050	$64 \times 65 \times 64$	$3\pi h \times 2h \times \pi h$	$295 \times (2.4 \sim 98) \times 98$	0.2	0.015

[1]Moser et al. (1999)
[2]Hoyas and Jiménez (2008)

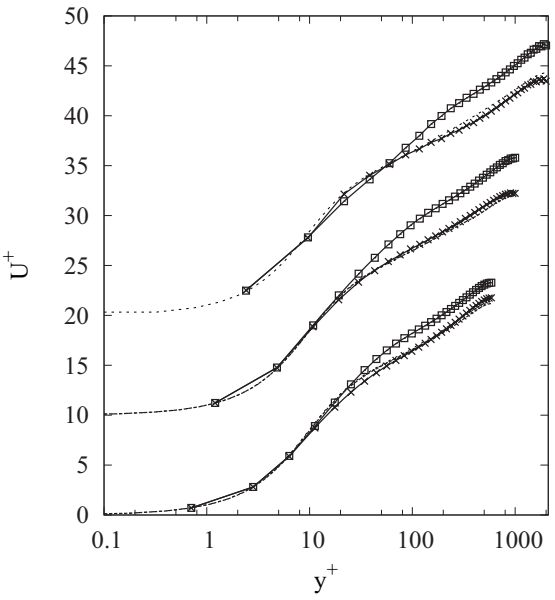

Figure 3: Streamwise mean velocity, for $Re_+ = 590$, $Re_+ = 1000$ and $Re_+ = 2000$ from bottom to top, respectively, shifted by 10 wall units upward. Square: LES; cross: LES-SSAM; dash: DNS (only for $Re_+ = 590$ and $Re_+ = 1000$); dots: DNS from Moser et al. (1999) for $Re_+ = 590$ and from Hoyas and Jiménez (2008) for $Re_+ = 1000$ and $Re_+ = 2000$.

by LES-SSAM are closer to DNS than in the classical LES. This result is mainly due to the fact that decorrelation is ensured by small scale fluctuations modelled with LESS-SSAM as seen by the spectra on fig. 6.

From figure 8 it can be seen that in agreement with the DNS, the distributions for components of the acceleration, a_i, obtained by LES-SSAM, present stretched tails, as a manifestation of intermittency, while these distributions from LES stay close to Gaussianity.

CONCLUSION

In the framework of the LES-SSAM approach, a new SGS model is proposed in order to represent the intermittency effects in the near-wall region of a high-Reynolds number channel flow. The assessment of this model is performed by comparison of computations with DNS data ($Re_+ = 590$, 1000 and 2000) and standard LES. The comparisons show explicitly the improvements of predictions provided by the new model.

ACKNOWLEDGMENTS

M. Buffat is acknowledged for the development of the computational code. Thanks to L. Faouzi who kindly provided his DNS fields. The numerical simulations reported here were performed at the Centre Informatique National de l'Enseignement Supérieur and at the Pôle de Compétence en Calcul Haute Performance Dédié.

REFERENCES

Adrian, R. J., Meinhart, C. D. and Tomkins, C. D., 2000, "Vortex organization in the outer region of the turbulent boundary layer", *Journal of Fluid Mechanics*, Vol. 422, pp. 1-54.

Dean, R. B., 1978, "Reynolds Number dependence on skin Friction and other bulk flow variables in two-dimensional rectangular duct flow", *Journal of Fluids Engineering*, Vol. 100, pp. 216-223.

Domaradzki, J. A. and Adams, N. A., 2002, "Direct modelling of subgrid scales of turbulence in large eddy simulations", *Journal of Turbulence*, Vol.3, pp. 0-24.

Gorokhovski, M. and Saveliev, V. L., 2008, "Statistical universalities in fragmentation under scaling symmetry with a constant frequency of fragmentation", *Journal of Physics D: Applied Physics*, vol. 41, pp. 085405.

Hoyas, S. and Jiménez, J., 2008, "Reynolds number effects on the reynolds-stress budgets in turbulent channels", *Physics of Fluids*, Vol. 20, pp. 101511.

Hutchins, N. and Marusic, I., 2007, "Evidence of very long meandering features in the logarithmic region of tur-

bulent boundary layers", *Journal of Fluid Mechanics*, Vol. 579, pp. 1-28.

Jiménez, J., Del Alamo, J. C. and Flores, O., 2004, "The large-scale dynamics of near-wall turbulence", *Journal of Fluid Mechanics*, Vol. 505, pp. 179-199.

Kaftori, D., Hetsroni, G. and Banerjee, S., 1994, "Funnel-shaped vortical structures in wall structures", *Physics of Fluids*, Vol. 6, pp. 3035-3050.

Kolmogorov, A. N., 1962, "A refinement of previous hypotheses concerning the local structure of turbulence in a viscous incompressible fluid at high Reynolds number", *Journal of Fluid Mechanics*, Vol. 13, pp. 82-85.

Lee, C., Yeo, K. and Choi, J.-I., 2004, "Intermittent nature of acceleration in near-wall turbulence", *Physical Review Letters*, Vol. 92.

Meneveau, C. and Katz, J., 2000, "Scale-invariance and turbulence models for large-eddy simulation", *Annual Reviews of Fluid Mechanics*, Vol. 32 pp. 1-32.

Mordant, N., Delour, J., Léveque, E. , Arnéodo, A. and Pinton, J.-F., 2002, "Long time correlations in lagrangian dynamics: a key to intermittency in turbulence", *Physical Review Letters* Vol. 89.

Mordant, Léveque, E. and Pinton, J.-F., 2004, "Experimental and numerical study of the Lagrangian dynamics of high Reynolds turbulence", *New Journal of Physics*, Vol. 6, pp. 116.

Moser, R. D., Kim, J. and Mansour, N. N., 1999 "Direct numerical simulation of turbulent channel flow up to $Re_\tau = 590$",*Physics of Fluids*, Vol. 11, pp. 943-945.

Oboukhov, A. M., 1962, "Some specific features of atmospheric tubulence", *Journal of Fluid Mechanics*, Vol. 13, pp. 77-81.

Park, N. and Mahesh, K., 2008, "A velocity-estimation subgrid model constrained by subgrid scale dissipation", *Journal of Computational Physics*, Vol. 227, pp.4190-4206.

Sabelnikov, V., Chtab, A. and Gorokhovski, M., 2007, "The coupled LES - sub-grid stochastic acceleration model (LES-SSAM", *Advances in Turbulence XI: Proceedings of the 11th EUROMECH European Turbulence Conference held June 25-28, 2007, in Porto, Portugal*, Springer Proceedings in Physics, pp. 209-211.

Sagaut, P., 2002, "Large Eddy Simulation for Incompressible Flows: An introduction", Springer Verlag, second ed.

Shur, M. L., Spalart, P. R., Strelets, M. K. and Travin, A. K., 2008, "A hybrid RANS-LES approach with delayed-DES and wall-modelled LES capabilities", *International Journal of Heat and Fluid Flow*, Vol. 26, pp. 1638.

Tomkins, C. D. and Adrian, R. J., 2003, "Spanwise structure and scale growth in turbulent boundary layers", *Journal of Fluid Mechanics*, Vol. 490, pp. 37-74.

Toh, S. and Itano, T., 2005, "Interaction between a large-scale structure and near-wall structures in channel flow", *Journal of Fluid Mechanics*, Vol. 524, pp. 249-262.

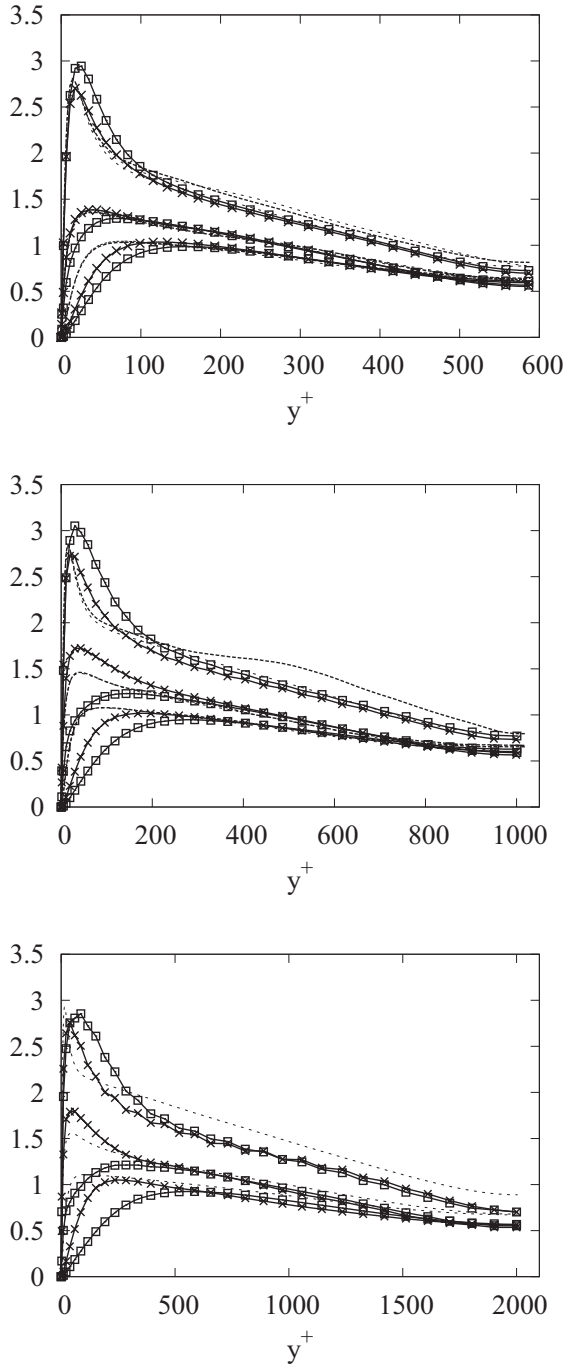

Figure 4: Standard deviation of streamwise (u), spanwise (w) and normal (v) velocity (in wall unites), for $Re_+ = 590$, $Re_+ = 1000$ and $Re_+ = 2000$, from top to bottom, respectively. Square: LES; cross: LES-SSAM; dash: DNS (only for $Re_+ = 590$ and $Re_+ = 1000$); dots: DNS from Moser et al. (1999) for $Re_+ = 590$ and from Hoyas and Jiménez (2008) for $Re_+ = 1000$ and $Re_+ = 2000$.

Sixth International Symposium on Turbulence and Shear Flow Phenomena
Seoul, Korea, 22-24 June 2009

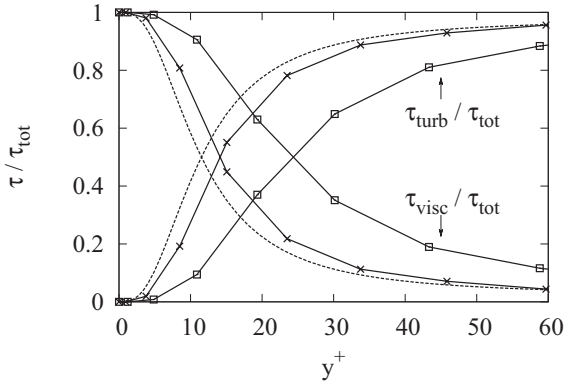

Figure 5: Fractions of turbulent $\tau_{turb} = -\rho\langle u'v'\rangle$ and viscous $\tau_{visc} = -\rho\nu\langle\frac{\partial u}{\partial y}\rangle$ stresses compared to the total one $\tau_{tot} = \tau_{visc} + \tau_{turb}$. $Re_+ = 1000$. Square: LES; cross: LES-SSAM; dash: DNS.

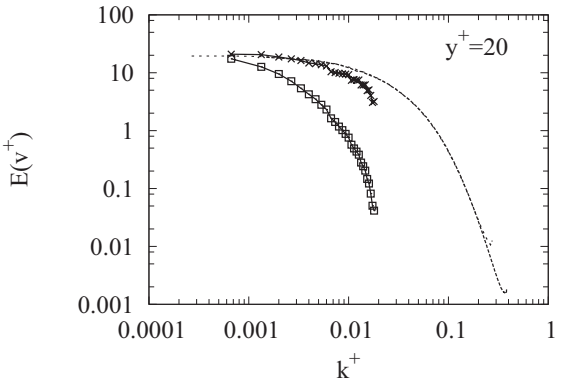

Figure 6: Normalized longitudinal 1-D spectra of normal to wall velocity for $y^+ = 20$ and $Re_+ = 1000$. Square: LES; cross: LES-SSAM; dash: DNS; dots: DNS from Hoyas and Jiménez (2008).

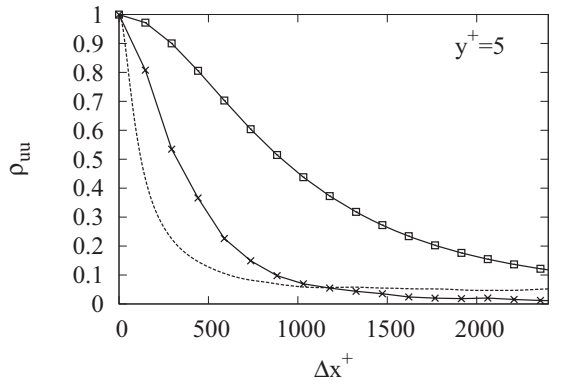

Figure 7: Longitudinal autocorrelation of streamwise velocity at $y^+ = 5$ and $Re_+ = 1000$. Square: LES; cross: LES-SSAM; dash: DNS.

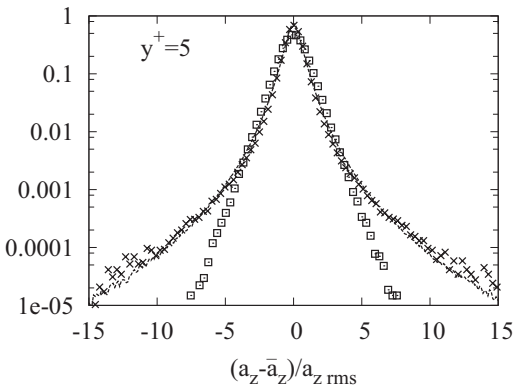

Figure 8: Distribution of spanwise acceleration at $y^+ = 5$ for $Re_+ = 1000$. Square: LES; cross: LES-SSAM; dash: DNS.